Catalytic Oxidation of H_2 by N_2O in the Gas Phase: O-Atom Transport with Atomic Metal Cations

Voislav Blagojevic,[†] Andrea Božović,[†] Galina Orlova,[‡] and Diethard K. Bohme*[,†]

Department of Chemistry, Centre for Research in Mass Spectrometry and Centre for Research in Earth and Space Science, York University, Toronto, Ontario, Canada M3J 1P3, and Department of Chemistry, St. Francis Xavier University, Antigonish, Nova Scotia, Canada B2G 2W5

Received: June 10, 2008; Revised Manuscript Received: July 25, 2008

Twenty-five atomic cations, M^+, that lie within the thermodynamic window for O-atom transport catalysis of the oxidation of hydrogen by nitrous oxide, have been checked for catalytic activity at room temperature with kinetic measurements using an inductively-coupled plasma/selected-ion flow tube (ICP/SIFT) tandem mass spectrometer. Only 4 of these 25 atomic cations were seen to be catalytic: Fe^+, Os^+, Ir^+, and Pt^+. Two of these, Ir^+ and Pt^+, are efficient catalysts, while Fe^+ and Os^+ are not. Eighteen atomic cations (Cr^+, Mn^+, Co^+, Ni^+, Cu^+, Ge^+, Se^+, Mo^+, Ru^+, Rh^+, Sn^+, Te^+, Re^+, Pb^+, Bi^+, Eu^+, Tm^+, and Yb^+) react too slowly at room temperature either in their oxidation with N_2O to form MO^+ or in the reduction of MO^+ by H_2. Many of these reactions are known to be spin forbidden and a few actually may lie outside the thermodynamic window. Three alkaline-earth metal monoxide cations, CaO^+, SrO^+, and BaO^+, were observed to favor MOH^+ formation in their reactions with H_2. A potential-energy landscape is computed for the oxidation of H_2 with N_2O catalyzed by $Fe^+(^6D)$ that vividly illustrates the operation of an ionic catalyst and qualitatively accounts for the relative inefficiency of this catalyst.

1. Introduction

Both experiment and theory are providing increasing insight into the kinetics of the homogeneous catalytic action of atomic metal cations in the gas-phase oxidation of small molecules by strong oxidants.[1,2] The fundamental steps of this type of catalysis involve the transport of an O atom by the metal cation from the oxidant to the substrate as illustrated in Scheme 1 for the gas-phase oxidation of unsaturated hydrocarbons.

The experiments are providing measurements of rate coefficients (and efficiencies) for the individual steps at room temperature, while molecular orbital computations are mapping out the appropriate potential energy landscapes for atomic-cation catalysis. This has been achieved, for example in our laboratory, for the oxidation of CO and unsaturated hydrocarbons by N_2O.[4,5] More emphasis now is given in the literature to the computation of energy landscapes for catalysis with atomic cations,[6−8] and polyatomic cationic and anionic catalysts comprised of metal clusters or mixed metal clusters are receiving increasing experimental and theoretical attention[1,9] Here, we provide extensive experimental results for the kinetics of the catalytic oxidation of hydrogen by nitrous oxide that is illustrated in Scheme 2, as well as some additional theoretical insight into the potential energy surface for this two-step process. The transformation of hydrogen to water of course is pivotal in current approaches to the conversion of chemical to electrical energy.

In previous experiments, we have thoroughly characterized the room temperature kinetics for the reduction of nitrous oxide by atomic metal cations according to reaction 1, the first leg in the catalytic cycle shown in Scheme 2. Using inductively-coupled plasma/selected-ion flow tube (ICP/SIFT) tandem mass spectrometry, we surveyed reactions of N_2O with 59 different atomic cations on the periodic table including third, fourth, and fifth row, as well as lanthanide, atomic cations.[10] Measurements of the kinetics of the second leg of the catalytic cycle, the oxidation of hydrogen to water indicated in reaction 2, have been sparse.

SCHEME 1: Catalytic Cycle for the Homogeneous Oxidation of Alkenes with Nitrous Oxide, Mediated by Atomic Alkaline-Earth Metal Cations[3]

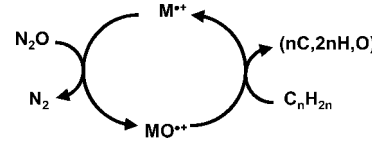

SCHEME 2: Catalytic Cycle for the Homogeneous Oxidation of Hydrogen with Nitrous Oxide, Mediated by Atomic Metal Cations

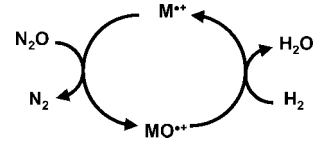

$$M^+ + N_2O \rightarrow MO^+ + N_2 \quad (1)$$

$$MO^+ + H_2 \rightarrow M^+ + H_2O \quad (2)$$

$$H_2 + N_2O \rightarrow H_2O + N_2 \quad (3)$$

The overall oxidation of H_2 by N_2O, according to reaction 3, involves the transfer of an O atom from N_2O to H_2.

Of the gas-phase reactions of metal monoxide cations with hydrogen, reaction 2, the reaction of FeO^+ has been explored in the greatest detail. This reaction has been investigated with

* Corresponding author. E-mail: dkbohme@yorku.ca.
[†] York University.
[‡] St. Francis Xavier University.

10.1021/jp805106d CCC: $40.75
Published on Web 09/20/2008

TABLE 1: Summary of the Measured Rate Coefficients for Reactions of Atomic Metal Cations, M^+, with N_2O To Produce MO^+ and Reactions of Metal-Monoxide Cations, MO^+, with H_2 and Catalytic Cycle Efficiencies for the Reduction of N_2O by H_2 Measured at Room Temperature Using an ICP/SIFT Tandem Mass Spectrometer and the Efficiencies for the Oxidation of M^+ by N_2O, E_{ox}, for the Reduction of MO^+ by H_2, E_{red}, and the Overall Efficiencies for the Catalytic Reduction of N_2O by H_2, E_{cycle}

M^+	$OA(M^+)$[a]	k_{ox}[b,c]	MO^+	k_{red}[b]	products	E_{ox}[c,d]	E_{red}[d]	E_{cycle}[e]
Ca^+	77.2	1.6×10^{-10}	CaO^+	7.0×10^{-12}	$CaOH^+$			
Cr^+	85.8 ± 2.8	1.5×10^{-13}	CrO^+	$<10^{-13}$				
Fe^+	80.0 ± 1.4	3.7×10^{-11}	FeO^+	8.75×10^{-12} [f]	Fe^+	0.043	4.4×10^{-3}	1.9×10^{-4}
Co^+	74.9 ± 1.2	1.1×10^{-12}	CoO^+	$<10^{-12}$				
Ge^+	81.8	3.6×10^{-10}	GeO^+	$<10^{-13}$				
Se^+	92	1.8×10^{-12}	SeO^+					
Sr^+	71.4	6.3×10^{-11}	SrO^+	3.0×10^{-12}	$SrOH^+$			
Ba^+	92.8	2.4×10^{-10}	BaO^+	1.6×10^{-13}	$BaOH^+$			
Re^+	115 ± 15	$<10^{-13}$	ReO^+					
Os^+	100 ± 12	2.3×10^{-11}	OsO^+	2.7×10^{-12}	Os^+	0.082	1.4×10^{-3}	1.1×10^{-4}
Ir^+	59	2.9×10^{-10}	IrO^+	7.7×10^{-10}	Ir^+	0.41	0.40	0.16
Pt^+	77	1.2×10^{-10}	PtO^+	1.1×10^{-9}	Pt^+	0.17	0.56	0.095
Eu^+	93.2 ± 4.3	6.9×10^{-11}	EuO^+	$<10^{-13}$				
Tm^+	116.6 ± 4.3	4.4×10^{-12}	TmO^+	$<10^{-13}$				
Yb^+	88.1 ± 5.9	6.5×10^{-13}	YbO^+	$<10^{-13}$				

[a] Oxygen-atom affinity in kcal mol^{-1} (see ref 10). [b] k is the reaction rate coefficient measured in units of cm^3 $molecule^{-1}$ s^{-1} with an certainty less than ±30%. [c] Previously published data from our laboratory.[10] [d] The efficiency, E, is defined as k/k_c, where k_c is the collision rate coefficient, calculated using the algorithm of the modified variational transition state/clasical trajectory theory developed by Su and Chesnavich.[28] [e] E_{cycle} is defined as $E_{ox} \times E_{red}$. The oxidation efficiencies, E_{ox}, for these metal cations have been previously published.[10] [f] Previously published data from our laboratory.[29]

multiple mass spectrometric techniques[11] as well as spin−orbit coupling[7a] and density functional[7b] calculations. The only channel that is observed experimentally is the production of Fe^+ by the reduction of FeO^+ which proceeds with a rate coefficients measured to be 1.6×10^{-11} cm^3 $molecule^{-1}$ s^{-1} with an FT-ICR instrument,[12] and 8.75×10^{-12} cm^3 $molecule^{-1}$ s^{-1} with a SIFT instrument at room temperature.[13] The relatively low rate of the reduction of FeO^+ by H_2, where the reaction rate is approximately 100× lower than the collision rate, has been attributed to the necessity of a crossing between the two spin states of the intermediate FeO^+/H_2 transition complex, a ground-state sextet and an excited-state quartet.[7]

The exothermic oxidation of H_2 by PtO^+ also has been measured to be rapid, $k = 5.0 \times 10^{-10}$ cm^3 $molecule^{-1}$ s^{-1},[14] although CoO^+ and NiO^+ both were observed to react with H_2 only very slowly with $k = 1.2 \times 10^{-12}$ and 2.1×10^{-12} cm^3 $molecule^{-1}$ s^{-1}, respectively, with the FT-ICR technique.[12] A guided-ion beam tandem mass spectrometer has been used to investigate cross sections for the onset with translational ion energy of the endothermic, spin forbidden oxidation of hydrogen by ScO^+, TiO^+, and VO^+.[15]

The oxidation of hydrogen by nitrous oxide, reaction 3, is exothermic by 76 kcal mol,[1,16] and this exothermicity defines the thermodynamic window for atomic ion catalysis.[4] The atomic metal ion must have an O-atom affinity high enough to abstract an O atom from N_2O and low enough to be able to then transfer the O atom to molecular hydrogen and make water, with both steps being exothermic. Here, we will explore the catalytic window for the oxidation of hydrogen by nitrous oxide for the 59 atomic cations that can now be routinely investigated in our laboratory with the ICP/SIFT tandem mass spectrometer.

2. Experimental Methods

The reactions were investigated in an inductively-coupled plasma/selected-ion flow tube (ICP/SIFT) tandem mass spectrometer. The apparatus has been described previously.[10,17,18] Elemental cations of interest are generated in an argon plasma operating at atmospheric pressure and approximately 5500 K. The plasma is fed with a dilute solution of salts containing the corresponding element. The ions generated in the plasma are introduced into a differentially pumped sampling interface, then mass selected by a quadrupole mass filter, and injected into a flow tube flushed with He buffer gas at 0.35 Torr and 295 ± 2 K. The atomic metal ions cool by radiation and collision with argon and helium from their point of origin in the ICP to the entrance of the reaction region. The state distribution of the ICP ions and their relaxation by collision and radiation before they reach the reaction region have been discussed in detail previously.[10] Neutral reagent molecules were added downstream into the reaction region. Ions present in the reacting mixtures were sampled by a second quadrupole mass spectrometer.

The metal oxide cations were produced by the reaction of the metal cation with N_2O that was added either directly into the flow tube upstream of the reaction region or into the prefilter region before the first quadrupole mass filter. When N_2O is added into the prefilter region, the monoxide cations that are formed are mass-selected by the first quadrupole mass filter before they are introduced into the flow tube. This latter method allows the measurement of rate coefficients for the monoxide cations in the absence of N_2O in the flow tube. The reactions of higher oxide cations are investigated by adding N_2O reagent gas directly upstream into the flow tube and then by adding H_2 into the reaction region. The occurrence of a catalytic cycle in the reaction region will prevent the determination of the rate coefficients for the reduction of oxide cations with H_2.

All measurements were performed at room temperature of 295 ± 2 K and at a helium operating pressure of 0.35 ± 0.01 Torr. The nitrous oxide was obtained commercially and was of high purity (Matheson Gas Products, >98.0%). The hydrogen was of C.P. grade (99.5%) and obtained from Canadian Liquid Air Ltd.

3. Computational Methods

We have performed a density functional theory (DFT) study of the reactions $N_2O + H_2 \rightarrow N_2 + H_2O$ (closed singlet), $Fe^+ + N_2O \rightarrow FeO^+ + N_2$ (sextet electronic state) and $FeO^+ + H_2 \rightarrow Fe^+ + H_2O$ (sextet electronic state). All theoretical predictions were made using the Gaussian03 program[19] with hybrid

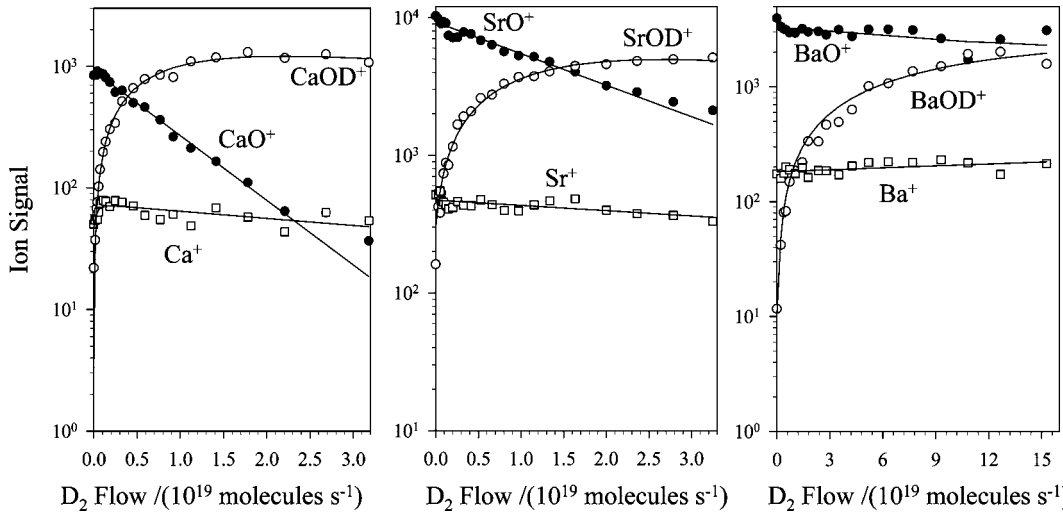

Figure 1. Reaction profiles measured for the reactions of CaO^+, SrO^+, and BaO^+ with D_2. The flows of N_2O are 1.6×10^{18}, 2.3×10^{18} and 2.8×10^{17} molecules s^{-1}, respectively. The Ca^+ signal has been corrected for overlap with Ar^+ and small amounts of deuterated water clusters, $H_xD_yO_2^+$, arising from water impurities in the helium buffer.

B3LYP[20,21] exchange-correlation functional. The 6−311++G(d,p) basis set [22,23] with diffuse and polarization functions [24,25] on hydrogen and heavy atoms was employed. Harmonic vibrational frequencies were computed to verify minima (all real frequencies) and transition state structures (one imaginary frequency). The connections between transition states and corresponding minima were verified using the intrinsic reaction coordinate technique (IRC) developed by Gonzalez and Schlegel.[26,27] Relative enthalpies at 0 K are reported. Cartesian coordinates and energetics in the Gaussian output format for all optimized structures are available as Supporting Information.

4. Results and Discussion

4.1. Thermodynamic Window for O-Atom Transport. The O-atom affinity of nitrogen to form nitrous oxide, $OA(N_2)$, is 39.95 ± 0.02 kcal mol^{-1} and that for H_2 to form H_2O, $OA(H_2)$, is 117.35 ± 0.02 kcal mol^{-1}.[16] This means that the "thermodynamic window of opportunity",[4] for the O-atom transport catalysis of reaction 3 is given by 40 kcal $mol^{-1} < OA(M^+) <$ 117 kcal mol^{-1}. Of the 59 atomic cations that can now be routinely investigated in our laboratory with the ICP/SIFT tandem mass spectrometer, 25 fall within this thermodynamic window within the uncertainties of their known O-atom affinities.[10] Four of these are borderline: $OA(Cu^+) = 37.4 \pm 3.5$, $OA(Mo^+) = 116.7 \pm 0.5$, $OA(Re^+) = 115 \pm 15$, and $OA(Tm^+) = 116.6 \pm 4.3$ kcal mol^{-1}.

4.2. Oxidation of Atomic Cations. The first leg of the catalytic cycle in which the atomic cation is oxidized with nitrous oxide, reaction 1, has been investigated in detail previously in our laboratory.[10] Of the 25 atomic cations that are within the thermodynamic window for the catalysis of interest in this study, only 15 were found to form monoxide cations according to reaction 1 with measurable rate coefficients, The known O-atom affinities of these 15 cations are included in Table 1 which also provides a summary of the observed kinetics.

The remaining 10 react very slowly, $k < 3 \times 10^{-12}$ cm^3 $molecule^{-1}$ s^{-1}, only to form adduct ions (Mn^+, Ni^+, Cu^+, Mo^+, Ru^+, Rh^+, Sn^+, Pb^+, and Bi^+) or not at all (Te^+). Low reactivities in exothermic O-atom transfer have been discussed previously, and these may be due to intrinsic activation barriers and spin constraints.[10]

4.3. Reduction of Monoxide Cations. Table 1 also includes a listing of the rate coefficients for the hydrogen reactions of the monoxide cations that could be generated from 13 of the atomic metal cations in the thermodynamic window and in sufficient amounts to allow a rate coefficient measurement (excluding ReO^+ and SeO^+).

Alkaline-Earth Oxide Cations. The alkaline earth metal monoxide cations, CaO^+, SrO^+, and BaO^+, were observed to favor formation of deuteroxide cations, XOD^+, according to reaction 4.

$$MO^+ + D_2 \rightarrow MOD^+ + D \quad (4)$$

The reactions are slow, $k = 7.0 \times 10^{-12}$, 3.0×10^{-12}, and 1.6×10^{-13} cm^3 $molecule^{-1}$ s^{-1}, respectively. Figure 1 shows data obtained for the reactions of CaO^+, SrO^+, and BaO^+ with D_2. D_2 was used rather than H_2 in order to improve the resolution of reactant and product ions with the analyzing quadrupole mass filter.

Both the reduction and the hydrogenation of these three metal oxide cations, reactions 5 and 7, are exothermic, with the latter being less exothermic, except for BaO^+.[16]

$$CaO^+ + H_2 \rightarrow CaOH^+ + H \quad \Delta_rH = -20 \text{ kcal mol}^{-1} \quad (5a)$$

$$\rightarrow Ca^+ + H_2O \quad \Delta_rH = -38.5 \text{ kcal mol}^{-1} \quad (5b)$$

$$SrO^+ + H_2 \rightarrow SrOH^+ + H \quad \Delta_rH = -28.4 \text{ kcal mol}^{-1} \quad (6a)$$

$$\rightarrow Sr^+ + H_2O \quad \Delta_rH = -36.4 \text{ kcal mol}^{-1} \quad (6b)$$

$$BaO^+ + H_2 \rightarrow BaOH^+ + H \quad \Delta_rH = -20 \text{ kcal mol}^{-1} \quad (7a)$$

$$\rightarrow Ba^+ + H_2O \quad \Delta_rH = -14.3 \text{ kcal mol}^{-1} \quad (7b)$$

Figure 1 shows no reduction of the alkaline earth oxide cations by hydrogen. So the hydrogen is not oxidized to water.

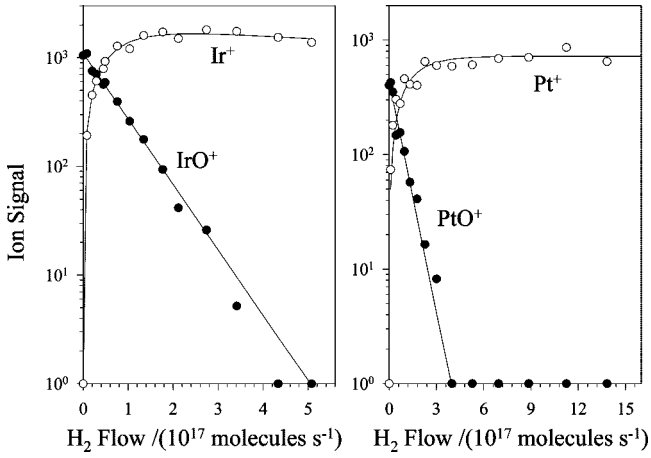

Figure 2. Reaction profiles recorded for the reactions of IrO^+ and PtO^+ with H_2. No N_2O was present in the flow tube.

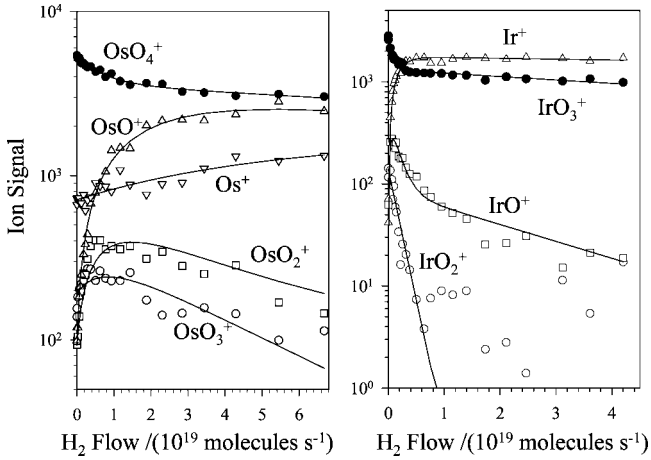

Figure 3. Reaction profiles measured for the reactions of OsO_n^+ and IrO_n^+ with H_2.The curvature in the decay of IrO_3^+ ion is not due to reverse reaction with N_2O but probably due to presence of two different isomers, one reactive and one unreactive. The flows of N_2O are 1.1×10^{18} and 3.3×10^{17} molecules s^{-1}, respectively.

It seems that the need to break the relatively strong H−H bond (104.2 kcal mol^{-1})[16] introduces a significant activation barrier for the water formation channel. On the other hand, hydroxide formation is a straightforward atom transfer reaction in which the gained in the formation of the H−H bond is offset by the energy gained in the formation of the O−H bond and is likely to proceed without an activation barrier. The reactions of CaO^+ and SrO^+ with H_2 are textbook examples of kinetically controlled reactions in which the observed products are kinetically favored rather than thermodynamically favored. Only with BaO^+ is the kinetically favored channel also thermodynamically more favorable.

Transition-Metal and Main Group Monoxide Cations. Reduction of the metal monoxide cations to bare metal cations according to reaction 2 was observed in experiments with FeO^+, OsO^+, IrO^+, and PtO^+. Measured ion profiles for the reactions of IrO^+ and PtO^+ cations are shown in Figure 2. Of the 4 monoxide cations that were observed to undergo reduction with H_2, FeO^+ ($E = 0.0045$) and OsO^+ ($E = 0.0014$) are slow, indicating a possible activation barrier to the reaction, while the reduction reactions with IrO^+ and PtO^+ proceed much more quickly, with efficiencies of 0.40 and 0.56, respectively. The previous FT-ICR result for FeO^+ of $k = 1.6 \times 10^{-11}$ cm^3 $molecule^{-1}$ s^{-1},[12] is higher by a factor of 1.8, and that for PtO^+, $k = 5.0 \times 10^{-10}$ cm^3 $molecule^{-1}$ s^{-1},[14] is lower by a factor of 2.2 than our SIFT results. These discrepancies lie within the combined experimental uncertainties. The value for CoO^+, $k = 1.2 \times 10^{-12}$ cm^3 $molecule^{-1}$ s^{-1},[12] is about the same, but we did not observe O-atom transfer.

The six monoxide cations, CrO^+, CoO^+, GeO^+, YbO^+, TmO^+, and EuO^+ did not react measurably with H_2 at the conditions of our experiments, $k < 10^{-13}$ cm^3 $molecule^{-1}$ s^{-1}.

OsO_n^+, IrO_n^+ and PtO_n^+. Several of the higher oxide cations of Os, Ir, and Pt also were found to be reduced by H_2. The oxide cations $OsO_{2,3,4}^+$, $IrO_{2,3}^+$, and $PtO_{2,3}^+$ all were found to be reduced by H_2 and to form the lesser oxide cation and water, sequentially according to reaction 8.

$$MO_n^+ + H_2 \rightarrow MO_{n-1}^+ + H_2O \quad (8)$$

OsO_4^+, IrO_3^+, and PtO_3^+ are reduced sequentially all the way to the bare metal cations. $PtO_2^+(N_2O)$ was observed to react with H_2 as well, producing PtO_2^+, N_2, and H_2O. Measured ion profiles that illustrate this chemistry are shown in Figure 3. The profile for IrO_3^+ shows a behavior similar to that we have observed previously in its reaction with CO and was attributed to the presence of two different isomers of IrO_3^+.[4] Reactions of hydrogen with OsO_n^+ cations were observed previously using FT-ICR mass spectrometry.[30] Reaction 9 was observed with $n = 1-3$ with $k = 0.07$, 3, and 0.01×10^{-10} cm^3 $molecule^{-1}$ s^{-1}, respectively, while reaction 10 was reported for OsO_4^+ with $k = 3 \times 10^{-10}$ cm^3 $molecule^{-1}$ s^{-1}. Because of the presence of N_2O in the reaction region of our flow tube experiments, we did not extract rate coefficients from the observed profiles since they are oxidized or solvated with N_2O.

$$OsO_n^+ + H_2 \rightarrow OsO_{n-1}^+ + H_2O \quad (9)$$

$$OsO_4^+ + H_2 \rightarrow OsO_4H^+ + H \quad (10)$$

4.4. Overall Catalytic Efficiencies. As regards the overall efficiency for the catalytic oxidation of H_2 by N_2O, the results are relatively disappointing, with only the catalytic oxidation with Ir^+ and Pt^+ being somewhat efficient ($E_{cycle} = 0.16$ and 0.095, respectively). The catalytic action of Os^+ is hampered by the slow reduction leg of the cycle ($E_{red} = 1.4 \times 10^{-3}$), while both legs of the cycle are inefficient ($E_{ox} = 0.043$, $E_{red} = 4.4 \times 10^{-3}$) in the case of Fe^+. A summary of the efficiencies for the reduction leg and the overall efficiencies of the cycles are included in Table 1.

4.5. Potential Energy Landscape for Catalysis. The potential-energy landscape computed for the oxidation of H_2 by N_2O catalyzed by $Fe^+(^6D)$ according to reactions 1 and 2 is shown in Figure 4. All of the intermediates and transition state structures on the catalyzed pathway are in the sextet electronic state. The uncatalyzed reduction shown in the top profile proceeds in one step via a high activation barrier of 55.0 kcal mol^{-1} and is strongly exothermic, by 73.4 kcal mol^{-1} according to the calculations and by 76 kcal mol^{-1} according to published enthalpies of formation.[16] The structure of the transition state, TS, corresponds to the insertion of the oxygen atom of N_2O into molecular hydrogen in a η^2-coordination. The N−O bond is being broken and the O−H bonds are being formed. The activation barrier for the catalyzed reduction of N_2O by H_2, apparently due to the cleavage of the N−O bond, is lowered by more than a factor of 50 to a mere 0.9 kcal mol^{-1} that arises in the first step of the much faster ionic path. The reaction coordinates of the ionic steps in this path are described by double and triple-minimum potential-energy profiles. The first step involves O-atom transfer from N_2O to Fe^+ with the formation of FeO^+ and N_2 and is described by a double-minimum potential

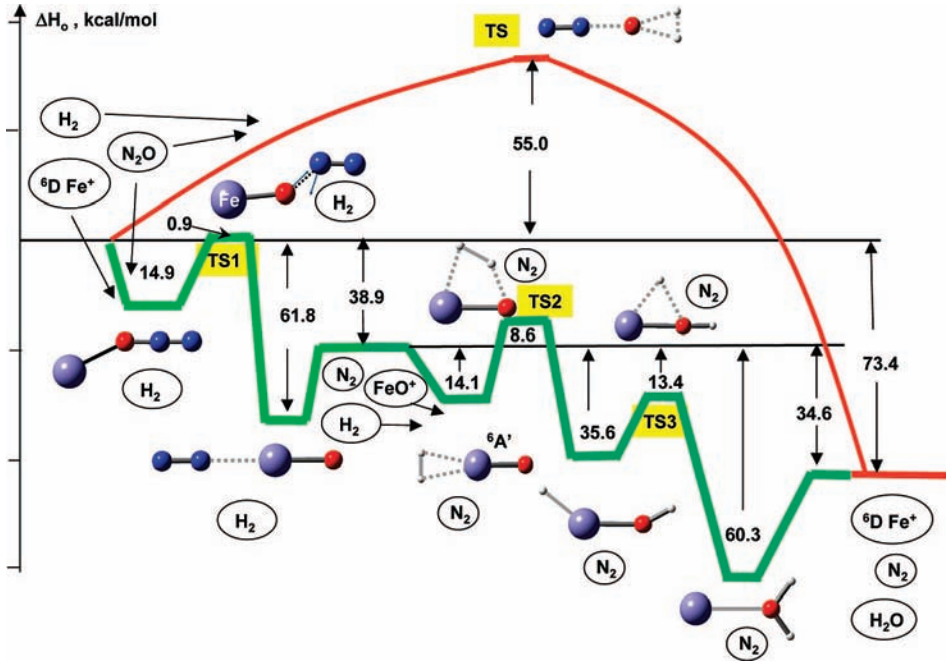

Figure 4. Energy landscape for the oxidation of H_2 by N_2O in the absence (red line) and presence (green lines) of Fe^+ (^6D) predicted using the B3LYP/6−311++G(d,p) method. The spectator molecules in each elementary step are circled.

energy profile. The activation barrier is 0.9 kcal mol^{-1} above the dissociation limit. This is somewhat lower than the barrier of 4.2 kcal mol^{-1} that we predicted recently[10a] using the B3LYP/SDD/6−311+G(d) method with the Stuttgart/Dresden[31] relativistic ECP and basis set, SDD, for iron. The higher value obtained might be attributable to the limitations[32] of the ECP and basis set that was used. The SDD also failed to predict the prereaction complex of FeO^+ with molecular hydrogen at the beginning of the second step of the catalyzed oxidation of H_2 by N_2O. This step involves O-atom transfer from FeO^+ to H_2 with the formation of Fe^+ and H_2O and proceeds on a triple-minimum profile. The energy of the rate-determining transition state, TS2, in this profile lies 8.6 kcal mol^{-1} above the dissociation limit to FeO^+ and H_2, and this is consistent with the small rate coefficient that was measured for the reaction of FeO^+ with H_2. The predicted reaction mechanism is also consistent with previous theoretical studies[7] at the MCSCF and DFT levels of theory which predicted a triple-minimum reaction profile with the barrier to the H−H cleavage as a rate-limiting step and similar relative energetics and geometries for the structures on this pathway.

5. Conclusions

Of the 25 candidate atomic metal cations, only four, Fe^+, Os^+, Ir^+, and Pt^+, were seen to catalyze the oxidation of H_2 by N_2O. Two of these, Ir^+ and Pt^+, are relatively efficient catalysts, while Fe^+ and Os^+ are not; in the case of Fe^+, both legs of the catalytic cycle, oxidation of the metal cation by N_2O and the reduction of the metal oxide cation by H_2, are slow. The potential-energy landscape computed for the oxidation of H_2 by N_2O catalyzed by Fe^+ (^6D) provides a clear picture of the mechanism and energetics of this catalysis, an explanation of the low catalytic efficiency of this metal cation, and another striking example of the extraordinary value of theoretical calculations in understanding catalytic cycles of this kind.[3,4,6−8] The oxide cations, $OsO_{1,2,3}^+$, $IrO_{1,2}^+$ and $PtO_{1,2}^+$, also were found to catalyze the oxidation of H_2 by N_2O, but quantitative measurements of the efficiency of these catalysts could not be made. However, the intermediate polyoxide cations, MO_n^+, were observed to be reduced by H_2 quite rapidly all the way to the bare metal cations, and this suggests that the oxides $OsO_{1,2,3}^+$, $IrO_{1,2}^+$ and $PtO_{1,2}^+$ are likely to be better catalysts than the corresponding bare atomic metal cations, especially Fe^+ and Os^+. Somewhat unexpectedly, alkaline earth metal monoxide cations formed metal hydroxide cations, XOH^+, in the reactions with H_2. Although in this case both reduction and hydroxide formation are exothermic, hydroxide formation is kinetically favored.

Acknowledgment. Continued financial support from the Natural Sciences and Engineering Research Council of Canada is greatly appreciated. Also, we acknowledge support from the National Research Council, the Natural Science and Engineering Research Council, and MDS SCIEX in the form of a Research Partnership grant. As holder of a Canada Research Chair in Physical Chemistry, Diethard K. Bohme thanks the contributions of the Canada Research Chair Program to this research.

Supporting Information Available: Electronic energies, enthalpies at 0 K and 298 K, Gibbs energies at 298 K, and Cartesians coordinates predicted for the reactions $N_2O + H_2 \rightarrow N_2 + H_2O$; $Fe^+ + N_2O \rightarrow FeO^+ + N_2$, and $FeO^+ + H_2 \rightarrow Fe^+ + H_2O$ (Figure 4) with the B3LYP/6−311++G(d,p) method. This material is available free of charge via the Internet at http://pubs.acs.org.

References and Notes

(1) Kappes, M. M.; Staley, R. H. *J. Am. Chem. Soc.* **1981**, *103*, 1286–1287.

(2) For a recent review see, for example Böhme, D. K.; Schwarz, H. *Angew. Chem., Int. Ed.* **2005**, *44*, 2336.

(3) Dažić, A.; Zhao, X.; Bohme, D. K. *Int. J. Mass Spectrom.* **2006**, *254*, 155–162.

(4) Blagojevic, V.; Orlova, G.; Bohme, D. K. *J. Am. Chem. Soc.* **2005**, *127*, 3545.

(5) Blagojevic, V.; Jarvis, M. J. Y.; Flaim, E.; Koyanagi, G. K.; Lavrov, V. V.; Bohme, D. K. *Angew. Chem., Int. Ed.* **2003**, *42*, 4923–4927.

(6) (a) Chiodo, S.; Russo, N.; Sicilia, E. *J. Comput. Chem.* **2005**, *26*, 175. (b) Rondinelli, F.; Russo, N.; Toscano, M. *Inorg. Chem.* **2007**, *46*, 7489.

(7) (a) Danovich, D.; Shaik, S. *J. Am. Chem. Soc.* **1997**, *119*, 1773. (b) Filatov, M.; Shaik, S. *J. Phys. Chem. A* **1998**, *102*, 3835.

(8) (a) Yoshizawa, K.; Shiota, Y.; Yamabe, T. *J. Am. Chem. Soc.* **1998**, *120*, 564. (b) Yoshizawa, K.; Shiota, Y.; Yamabe, T. *J. Chem. Phys.* **1999**, *111*, 538. (c) Shiota, Y.; Yoshizawa, K. *J. Am. Chem. Soc.* **2000**, *122*, 12317. (d) Shiota, Y.; Yoshizawa, K. *J. Chem. Phys.* **2003**, *118*, 5872. (e) Yoshizawa, K.; Shiota, Y.; Kagawa, Y; Yamabe, T. *J. Phys. Chem. A* **2000**, *104*, 2552.

(9) (a) See, for example, Wallace, W. T.; Whetten, R. L. *J. Am. Chem. Soc.* **2002**, *124*, 7499. (b) Kimble, M. L.; Moore, N. A.; Castleman, A. W., Jr.; Buergel, C.; Mitric, R.; Bonacic-Koutecky, V. *Eur. Phys. J. D: Atomic, Molecular, Optical and Plasma Phys.* **2007**, *43*, 205. (c) Buergel, C.; Reilly, N. M.; Johnson, G. E.; Mitric, R.; Kimble, M. L.; Castleman, A. W.; Bonacic-Koutecky, V. *J. Am. Chem. Soc.* **2008**, *130*, 1694. (d) Adlhart, C.; Uggerud, E. *Chem. Eur. J.* **2007**, *13*, 6883M. (e) Hanmura, T.; Ichihashi, M.; Watanabi, Y.; Isomura, N.; Kondow, T. *J. Phys. Chem. A* **2007**, *111*, 422.

(10) (a) Lavrov, V. V.; Blagojevic, V.; Koyanagi, G. K.; Orlova, G.; Bohme, D. K. *J. Phys. Chem. A* **2004**, *108*, 5610. (b) Koyanagi, G. K.; Bohme, D. K. *J. Phys. Chem. A* **2001**, *105*, 8964.

(11) Schröder, D.; Schwarz, H.; Clemmer, D. E.; Chen, Y.; Armentrout, P. B.; Baranov, V. I.; Bohme, D. K. *Int. J. Mass Spectrom. Ion Processes* **1997**, *161*, 175.

(12) Schröder, D.; Fiedler, A.; Ryan, M. F.; Schwarz, H. *J. Phys. Chem.* **1994**, *98*, 68.

(13) Baranov, V.; Javahery, G.; Hopkinson, A. C.; Bohme, D. K. *J. Am. Chem. Soc.* **1995**, *117*, 12801.

(14) Brönstrup, M.; Schröder, D.; Kretzschmar, I.; Schwarz, H.; Harvey, J. N. *J. Am. Chem. Soc.* **2001**, *123*, 142.

(15) Clemmer, D. E.; Aristov, N.; Armentrout, P. B. *J. Phys. Chem.* **1993**, *97*, 544.

(16) Lias, S. G.; Bartmess, J. E.; Liebman, J. F.; Holmes, J. L.; Levin, R. D.; Mallard, W. G. *J. Phys. Chem. Ref. Data* **1988**, *17*, Supplement 1.

(17) Koyanagi, G. K.; Lavrov, V. V.; Baranov, V.; Bandura, D.; Tanner, S.; McLaren, J. W.; Bohme, D. K. *Int. J. Mass Spectrom.* **2000**, *194*, L1.

(18) Koyanagi, G. K.; Baranov, V. I.; Tanner, S. D.; Bohme, D. K. *J. Anal. Atom. Spectrom.* **2000**, *15*, 1207.

(19) Frisch, M. J.; Trucks, G. W.; Schlegel, H. B.; Scuseria, G. E.; Robb, M. A.; Cheeseman, J. R.; Montgomery, J. A., Jr.; Vreven, T.; Kudin, K. N.; Burant, J. C.; Millam, J. M.; Iyengar, S. S.; Tomasi, J.; Barone, V.; Mennucci, B.; Cossi, M.; Scalmani, G.; Rega, N.; Petersson, G. A.; Nakatsuji, H.; Hada, M.; Ehara, M.; Toyota, K.; Fukuda, R.; Hasegawa, J.; Ishida, M.; Nakajima, T.; Honda, Y.; Kitao, O.; Nakai, H.; Klene, M.; Li, X.; Knox, J. E.; Hratchian, H. P.; Cross, J. B.; Bakken, V.; Adamo, C.; Jaramillo, J.; Gomperts, R.; Stratmann, R. E.; Yazyev, O.; Austin, A. J.; Cammi, R.; Pomelli, C.; Ochterski, J. W.; Ayala, P. Y.; Morokuma, K.; Voth, G. A.; Salvador, P.; Dannenberg, J. J.; Zakrzewski, V. G.; Dapprich, S.; Daniels, A. D.; Strain, M. C.; Farkas, O.; Malick, D. K.; Rabuck, A. D.; Raghavachari, K.; Foresman, J. B.; Ortiz, J. V.; Cui, Q.; Baboul, A. G.; Clifford, S.; Cioslowski, J.; Stefanov, B. B.; Liu, G.; Liashenko, A.; Piskorz, P.; Komaromi, I.; Martin, R. L.; Fox, D. J.; Keith, T.; Al-Laham, M. A.; Peng, C. Y.; Nanayakkara, A.; Challacombe, M.; Gill, P. M. W.; Johnson, B.; Chen, W.; Wong, M. W.; Gonzalez, C.; Pople, J. A. *Gaussian 03, Revision C.02*; Gaussian, Inc.: Wallingford, CT, 2004.

(20) Becke, A. D. *J. Chem. Phys.* **1993**, *98*, 5648.

(21) Lee, C.; Yang, W.; Parr, R. G. *Phys. Rev. B* **1988**, *37*, 785.

(22) Hehre, W. J.; Ditchfield, R.; Pople, J. A. *J. Chem. Phys.* **1972**, *56*, 2257.

(23) Krishnan, R.; Binkley, J. S.; Seeger, R.; Pople, J. A. *J. Chem. Phys.* **1980**, *72*, 650.

(24) Chandrasekhar, J.; Andrade, J. G.; Schleyer, P. v. R. *J. Am. Chem. Soc.* **1981**, *103*, 5609.

(25) Clark, T.; Chandrasekhar, J.; Spitznagel, G. W.; Schleyer, P. v. R. *J. Comput. Chem.* **1983**, *4*, 294.

(26) Gonzalez, C.; Schlegel, H. B. *J. Chem. Phys.* **1989**, *90*, 3154.

(27) Gonzalez, C.; Schlegel, H. B. *J. Phys. Chem.* **1990**, *94*, 5523.

(28) Su, T.; Chesnavich, W. J. *J. Chem. Phys.* **1982**, *76*, 5183.

(29) (a) Baranov, V.; Javahery, G.; Hopkinson, A. C.; Bohme, D. K. *J. Am. Chem. Soc.* **1995**, *117*, 12801. (b) Schröder, D.; Schwarz, H.; Clemmer, D. E.; Chen, Y.; Armentrout, P. B.; Baranov, V. I.; Bohme, D. K. *Int. J. Mass Spectrom. Ion Processes* **1997**, *161*, 175.

(30) Irikura, K. K.; Beauchamp, J. L. *J. Am. Chem. Soc.* **1989**, *111*, 75.

(31) Dolg, M.; Wedig, U.; Stoll, H; Preuss, H. *J. Chem. Phys.* **1987**, *86*, 866.

(32) Fuentealba, P.; Savin, A. *J. Phys. Chem. A* **2000**, *104*, 10882.

JP805106D